European Review for Medical and Pharmacological Sciences 2022; 26: 7938-7948

Diagnostic performance of MRI perfusion and spectroscopy for brainstem glioma grading

D. TRAN[1,2], D.-H. NGUYEN[3,4], H.-K. NGUYEN[3], V.-A. NGUYEN-THANH[3], H. DONG-VAN[1], M.-D. NGUYEN[5]

[1]Neurosurgery Center, Viet Duc Hospital, Hanoi, Vietnam
[2]Department of Surgery, Hanoi Medical University, Hanoi, Vietnam
[3]Department of Radiology, Hanoi Medical University, Hanoi, Vietnam
[4]Department of Radiology, Viet Duc Hospital, Hanoi, Vietnam
[5]Department of Radiology, Pham Ngoc Thach University of Medicine, Ho Chi Minh City, Vietnam

Abstract. – OBJECTIVE: This study investigated the roles of dynamic susceptibility contrast (DSC) perfusion and multivoxel magnetic resonance spectroscopy (MRS) in grading brainstem glioma (BSG).

PATIENTS AND METHODS: Our retrospective study comprised 12 patients, including 6 with pathology verified low-grade BSGs and 6 with high-grade BSGs. We examined differences in age, relative cerebral blood volume (rCBV), regional cerebral blood flow (rCBF), and the metabolite ratios of choline (Cho)/N-acetyl aspartate (NAA) and Cho/creatine (Cr) between these two groups using the Mann-Whitney U test and Chi-square test. Receiver operating characteristic (ROC) curve analysis was used to establish cutoff values and assess their usefulness in grading BSG.

RESULTS: The Cho/NAA metabolite ratio had the strongest preoperative predictive performance for identifying the correct histological grade among BSGs, with an area under the ROC curve (AUC) value of 0.944 (cutoff: 3.88, sensitivity [Se]: 83.3%; specificity [Sp]: 100%), followed by the Cho/Cr ratio (cutoff: 3.08; AUC: 0.917; Se: 83.3%; Sp: 100%), rCBF (cutoff: 3.56, AUC: 0.917; Se: 83.3%; Sp: 100%), rCBV (cutoff: 3.16, AUC: 0.889; Se: 100%; Sp: 66.7%), and age (cutoff: 9.5 years, AUC: 0.889; Se: 100%; Sp: 83.3%).

CONCLUSIONS: rCBF and rCBV values comparing solid tumors with the normal brain parenchyma and the metabolite ratios for Cho/NAA and Cho/Cre may serve as useful indices for establishing BSG grading and provide important information when determining treatment planning and prognosis in patients with BSG.

Key Words:
Dynamic susceptibility contrast, Perfusion, Spectroscopy, Brainstem glioma, Grading.

Introduction

Brainstem gliomas (BSGs) account for 10% of all brain tumors in children and 2% of all brain tumors in adults[1-3]. BSG describes a heterogeneous group of gliomas that vary significantly in histology and prognosis. According to the fifth edition of the WHO classification of central nervous system (CNS) tumors, published in 2021, gliomas can be classified from grade I to IV[4]. In BSG, the histological grade plays a crucial role in treatment planning and is significantly associated with overall survival[5-8]. Pathology is the gold standard for diagnosing BSG at the cellular level, based on the detection of necrosis, nuclear polymorphism, and endothelial proliferation. However, the performance of biopsies or surgery to characterize or treat brainstem tumors is both challenging and controversial due to the high risks of complications and mortality[9].

Magnetic resonance imaging (MRI) allows for the noninvasive diagnosis of BSG. MRI can provide a definitive diagnosis in cases of typical diffuse midline glioma, and many brainstem tumors are diagnosed and treated based on imaging findings without histological results[10,11]. Although the value of MRI for BSG prognosis has been mentioned in prior studies, few studies have examined the role of MRI in BSG grading, which is typically performed using conventional approaches, with a sensitivity (Se) of 46.6% and a specificity (Sp) of 96%[9,10]. Advanced MRI approaches, such as the combination of magnetic resonance perfusion (MRP), particularly dynamic susceptibility contrast (DSC) perfusion, and magnetic resonance spectroscopy (MRS), have been widely used to investigate the extent of angiogenesis and tumor

Corresponding Authors: Nguyen Duy Hung; e-mail: bsnguyenminhduc@pnt.edu.vn
Nguyen Minh Duc; e-mail: bsnguyenminhduc@pnt.edu.vn

metabolism, factors that are closely correlated with BSG malignancy. However, very few studies have evaluated the role of these sequences in BSG grading, and no studies have reported cutoff values for indicators measured using DSC perfusion or MRS. Therefore, we examined the role of DSC perfusion and MRS in BSG grading and established cutoff values for various indices used in the differential diagnosis of low-grade BSG (BS-LGG) from high-grade BSG (BS-HGG).

Patients and Methods

Study Population

This retrospective study was conducted in the Viet Duc University Hospital Radiology Department, covering the period from June 2019 to May 2022. Twelve enrolled patients (6 with BS-LGG and 6 with BS-HGG) were examined using 3.0 Tesla MRI (SIGNA Pioneer MR, GE Healthcare, Chicago, IL, USA), using the same protocol for all patients (described in Table I) consisting of both conventional and DSC perfusion and multivoxel MRS. All patients subsequently underwent surgery or stereotactic biopsy to obtain a sample for pathological glioma confirmation. The exclusion criteria were patients who received any treatment prior to MRI assessment, such as operative resection, biopsy, or cranial radiotherapy; and patients with MRI results of poor quality, such as the presence of motion artifacts that prevented accurate measurements. This study was reviewed and approved by the Institutional Review Board (Ref: 634/GCN-HDDDNCYSH-DHYHN dated 16 March 2022). Our retrospective study was performed in compliance with the principles outlined in the Declaration of Helsinki. The requirement for informed consent from children and their parents/guardians was waived by the Institutional Review Board of Hanoi Medical University due to the retrospective study, which analyzed anonymized imaging data.

MRI Technique

All research subjects underwent brain MRI evaluations using a 3.0 Tesla scanner system (SIGNA Pioneer MR, GE Healthcare, Chicago, IL, USA) with head coils; the protocol applied to all patients is presented in Table I. Due to the need for prolonged assessments, sedation or general anesthesia is typically necessary to obtain good quality images in children younger than 6 years and some patients with altered mental status. The need for sedation should be assessed on a case-by-case basis. Informed consent was obtained from patients or their parents/guardians for the use of sedation or general anesthesia, and all consents were documented and stored. DSC perfusion was obtained before the administration of contrast agent and the collection of T1-weighted (T1W) contrast images.

Table I. MRI sequences.

Sequence	Plane	TR (msec)	TE (msec)	Thickness (mm)	Matrix	FOV	Others
FLAIR	Axial	8500	117	5	184 × 256	240 × 240	IR 2500 ms
T2 TSE	Axial, coronal	2500	100	5	360 × 288	220 × 220	
T2*/SWI							†
T1 SE	Axial, sagittal	2325	24	5	240 × 240	300 × 224	
T1 SE CE+	Axial, sagittal	2325	24	5	240 × 240	300 × 224	‡
DSC-MRI	GRE EPI	1250	45	5	88 × 87	338 × 240	§
MRS	2D multivoxel CSI	8500	144			240 × 240	
	Voxel 3D CSI	2000	144		Voxel size of 0.9 × 1.6 × 1.2 cm^3		

TR: Repetition time; TE: Echo time; FOV: Field of view; FLAIR: Fluid-attenuated inversion recovery; IR: Inversion time; T2 TSE: T2-weighted turbo spin-echo; SWI: Susceptibility-weighted imaging; T1 SE: T1-weighted spin-echo; CE+: Contrast enhancement; DSC-MRI: Dynamic susceptibility contrast perfusion magnetic resonance imaging; GRE EPI: gradient-recalled echo-planar imaging; CSI: chemical shift imaging; MRS, magnetic resonance spectroscopy. †Optimal sequence (T2* or SWI) for each patient. ‡Intravenous injection of contrast agent (gadolinium–diethylenetriamine pentaacetate [DTPA] at 1 ml/kg, with an injection rate of 5 mL/s). §Performed before T1-SE CE+ during the first pass of an intravenous bolus injection of contrast agent (gadolinium–DTPA at 1 ml/kg, with an injection rate of 5 mL/s), 40 acquisition scans with voxel size 2.5 × 2.5 × 5 mm. DSC-MRI was performed using the dynamic T2*-weighted GRE EPI. MRS was performed using 2D multivoxel CSI and Voxel 3D CSI.

Image Analysis

MRI results were interpreted according to current radiological criteria by a neuroradiologist with more than 10 years of experience in a blinded manner, with no knowledge of the pathological results, clinical findings, or previous imaging findings. The following regions (Figure 1) were established using the conventional MRI results:

1. Solid tumor regions were defined as enhanced sites on T1W contrast-enhanced MRI.
2. Normal brain parenchyma was defined as normal contralateral white matter in the cerebral hemisphere or middle cerebral peduncle from the same images used to define the solid tumor.
3. Cystic degenerating or necrotic tumor regions were defined as regions with significant hypointensity on T1W images and hyperintensity on T2W images, with no contrast enhancement.
4. Intratumoral calcifications and hemorrhagic regions were defined as areas that displayed signal drop-out or blooming artifacts on T2* or post-processed susceptibility-weighted imaging (SWI) and appeared hyperdense on computed tomography images (if available).

Locations containing signals that might interfere with the accurate assessment of signal intensity for the region of interest (ROI) or the voxel placing region were excluded from further analysis (referred to as artifact regions), such as any regions containing tumoral cystic degeneration, calcifications, hemorrhagic regions, intratumoral necrosis, or intratumor vessels. Areas near the skull bone, subcutaneous adipose tissue, and regions with significant variations in magnetic susceptibility were also excluded from the analysis.

MRS was performed for each patient using two-dimensional (2D) multivoxel chemical shift imaging (CSI) or single-voxel 3-dimensional (3D) CSI to identify and quantify metabolites in both the normal brain parenchyma and the intratumoral solid regions. For each patient, a freehand ROI (diameter of 3-4 mm) was manually drawn on a single axial slide containing both the solid tumor and the normal parenchyma free of artifacts (Figure 2). Spectroscopic analysis showed measured the following metabolites: N-acetyl aspartate (NAA) at 2.18-2.01 ppm; creatine (Cr) at 3.15–3.0 ppm; and choline (Cho) at 3.36-3.21 ppm. The Cho/Cr and Cho/NAA ratios were automatically calculated by the software using the integration values of each metabolite in the same spectrum.

The DSC perfusion sequence was acquired during the first pass of a bolus contrast injection, before contrast-enhanced T1W was performed, using dynamic T2*-weighted gradient-recall echo-planar imaging with the same slide thickness as the fluid-attenuated inversion recovery (FLAIR) or T2-weighted (T2W) axial sequence

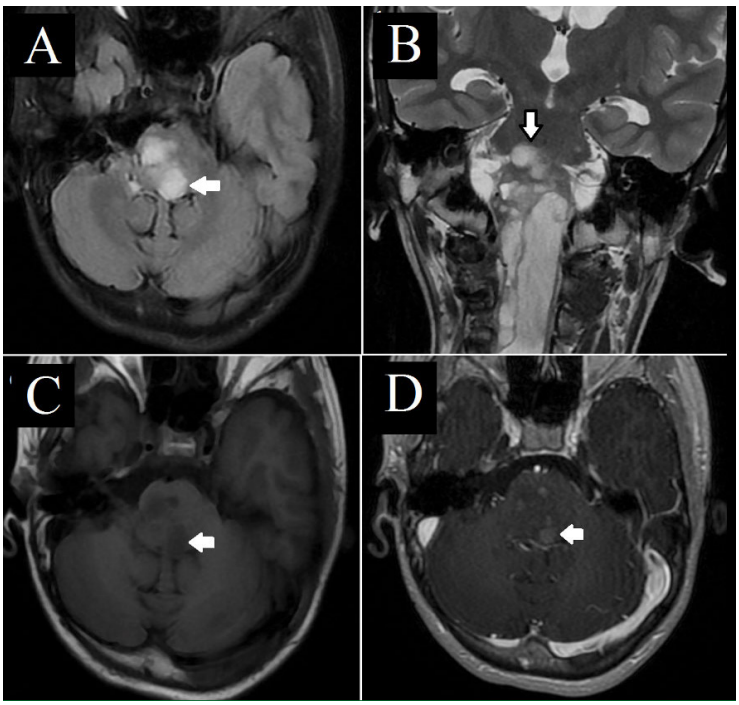

Figure 1. A 14-year-old male patient presented with a mild headache for 4 months. Axial fluid-attenuated inversion recovery (**A**) and coronal T2-weighted images (**B**) show a heterogenous, hyperintense mass (white arrows) in the brainstem that extends to the upper cervical spine, causing cystic collection in the central canal of the spinal cord, known as syringomyelia. Axial T1-weighted (**C**) and axial T1-weighted contrast-enhanced (**D**) imaging at the same level manifest faint heterogeneous enhancement *(white arrows)*.

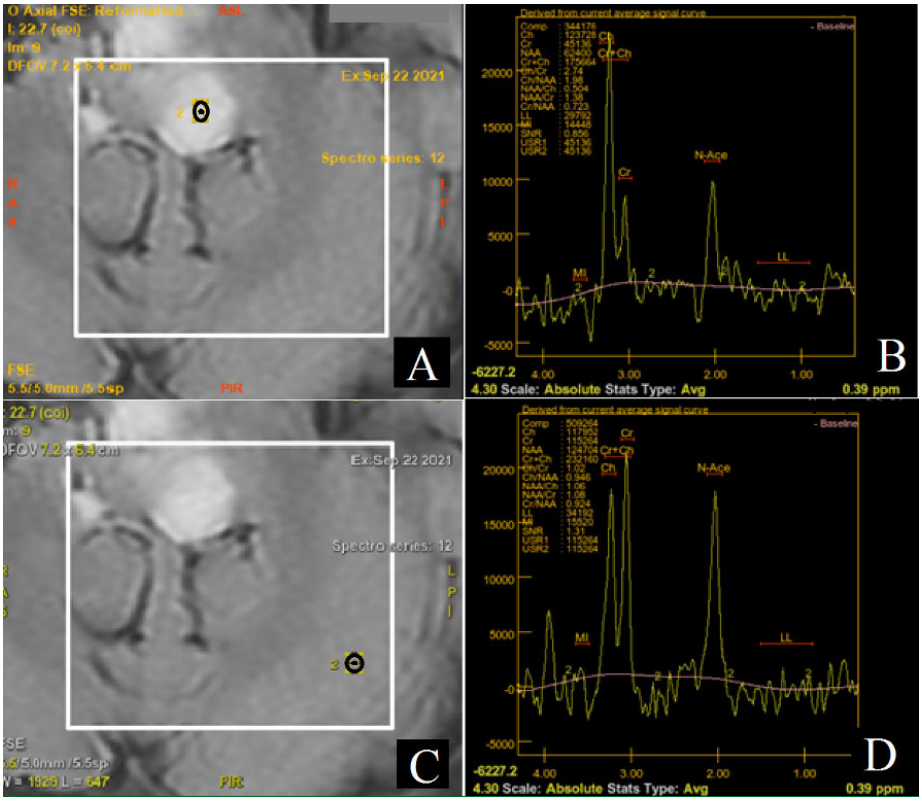

Figure 2. A 14-year-old male patient presented with a mild headache for 4 months. The images presented here were obtained at the same level as in Figure 1. MR spectroscopy was conducted using 2-dimensional multivoxel chemical shift imaging in both solid tumor regions (**A-B**) and the normal brain parenchyma (**C-D**) using ROIs (the black circles in **A** and **C**) to estimate the integral values of each metabolite. The choline/N-acetyl aspartate and choline/creatine ratios were calculated automatically.

to assist the juxtaposition of the perfusion results with other pre-contrast sequences. Phase encoding was performed in the anterior-posterior direction for all patients to reduce susceptibility artifacts. The obtained cerebral blood volume (CBV) and cerebral blood flow (CBF) maps were used for further analyses. Two ROIs (diameter of 3-5 mm) were drawn on the solid tumor and normal brain parenchyma at the same level to measure the CBV and CBF values. The selected tumor region was the most hypervascular area that manifested "hot spot areas" of great intensity on the CBV color map, excluding artifact areas. Hemodynamic parameters were calculated from the concentration-time curves, including relative cerebral blood volume (rCBV) and regional cerebral blood flow (rCBF), by normalizing the maximum values obtained for the solid tumor by the values obtained for the normal brain parenchyma (Figure 3).

Histopathological Examination

All patients underwent surgery or stereotactic biopsy to obtain a sample for histopathology, which was used to confirm glioma diagnosis. According to the WHO categorization, and to facilitate our statistical analysis, patients were classified as either BS-LGG (WHO grades I and II) or BS-HGG (WHO grades III and IV).

Statistical Analysis

Data were analyzed using SPSS 20.0 (Statistical Package for Social Sciences version 20.0, SPSS Inc., Armonk, NY, USA) to determine correlations between MRI characteristics and pathological features. Each parameter was calculated and presented as the mean with both the 25th and 75th percentiles (Q1-Q3) and the standard deviation (SD). Differences between the BS-LGG and BS-HGG were evaluated using the Mann-Whitney U test for age, rCBV, rCBF, Cho/NAA, and Cho/Cre. Categorical variables were compared using the Chi-square test or Fisher's exact test. The *p*-values lower than 0.05 were considered significant. Receiver operating characteristic (ROC) curve analysis was performed to estimate the optimal cutoff values for each parameter by maximizing the sum of Se and Sp using the Youden Index. The area under the ROC curve (AUC) was also determined.

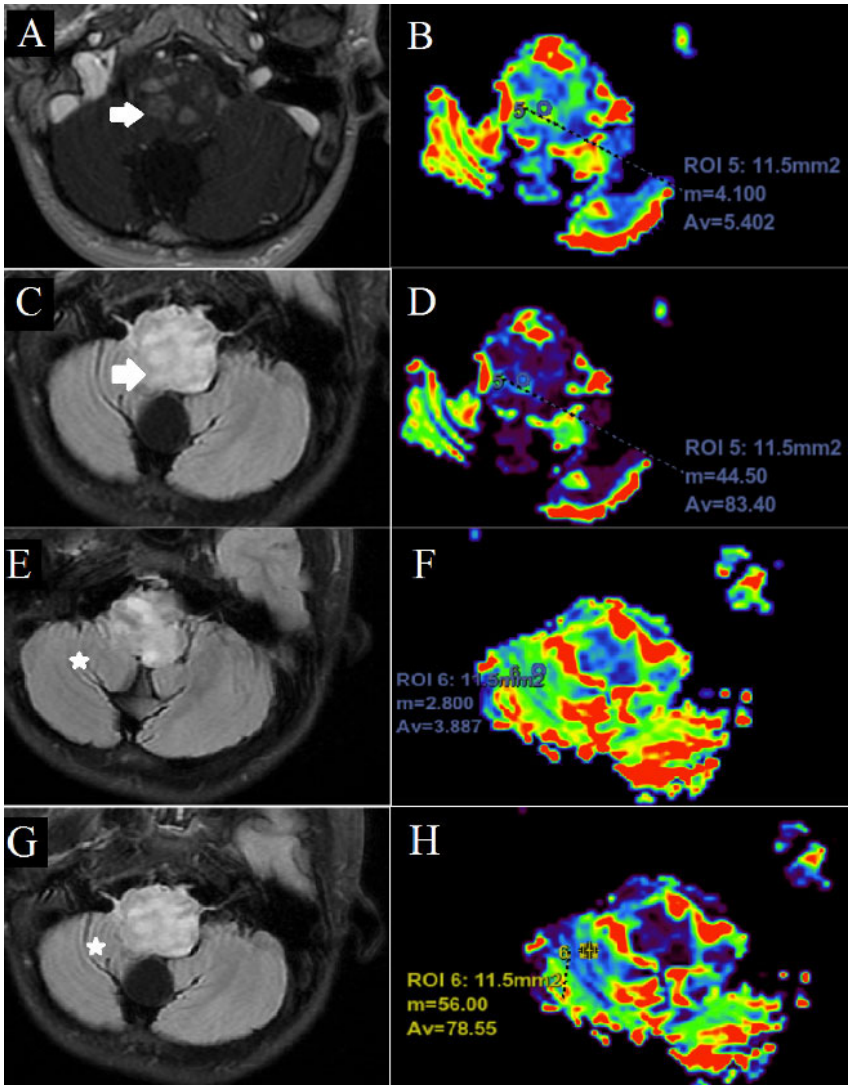

Figure 3. A 14-year-old male patient presented with a mild headache for 4 months. This image presents an analysis of the same patient from Figure 1 at a lower level, where the tumor manifests "hot spots" on the cerebral blood volume (CBV) color map compared with the normal white matter parenchyma of the cerebellum. Axial T1-weighted contrast-enhanced (**A**) and axial fluid-attenuated inversion recovery (FLAIR, **B**) imaging show a diffuse mass in the brainstem (white arrows). The tumoral ROI was placed to capture the greatest intensity on the CBV (**B**) and cerebral blood flow (CBF) maps (**D**). Axial FLAIR (**E-G**) images at the same level show the normal white matter parenchyma (stars) used for placing ROIs on the CBV (**F**) and CBF maps (**H**).

Results

The study population included 12 patients (6 males and 6 females; 7 pediatric patients and 5 adults), 6 of whom were diagnosed with BS-LGG and 6 of whom were diagnosed with BS-HGG. The BS-LGG group included 5 patients diagnosed with WHO grade I and 1 patient diagnosed with WHO grade II BSG, whereas the BS-HGG group included 1 patient diagnosed with WHO grade III and 5 patients diagnosed with WHO grade IV BSG. Details are provided in Table II. The demographic characteristics, rCBV, rCBF, Cho/NAA, and Cho/Cr values for the entire cohort are summarized in Table III. No significant difference in sex distribution (p = 0.248) was identified between the two groups. Strong correlations were identified between age, rCBV, rCBF, Cho/NAA, and Cho/Cr values and tumor malignancy among BSG patients. The mean age of the BS-HGG group (14.8 ± 17.8 years) was significantly lower than that of the BS-LGG group (35.5 ± 22.9 years, p = 0.024). The mean rCBV, rCBF, Cho/NAA, and Cho/Cr values were significantly higher for the BS-HGG group than for the BS-LGG group (Table III).

Table II. Detailed histopathological diagnoses of the studied cases.

Pathological diagnosis	Grade	Number of cases	Percentage
Pilocytic astrocytoma	I	3	25
Diffuse astrocytoma	I	2	17
Pilomyxoid astrocytoma	II	1	8
Anaplastic astrocytoma	III	1	8
Diffuse midline glioma	IV	5	42
Total		**12**	**100**

Table III. Descriptive statistics for high-grade and low-grade brainstem gliomas according to demographic characteristics, MR spectroscopy, and MR perfusion data.

Parameter	Low-grade glioma n = 6	High-grade glioma n = 6	*p*-value
Sex (male/female)	4/2	2/4	0.248[a]
Age, years	35.5 ± 22.9	14.8 ± 17.8	0.024[b]
Q1-Q3	13-58	6-19.5	
rCBV	2.77 ± 1.33	8.53 ± 6.21	0.025[b]
Q1-Q3	1.32-3.59	3.19-14.22	
rCBF	2.27 ± 1.27	7.97 ± 4.67	0.016[b]
Q1-Q3	0.98-3.49	3.34-12.12	
Cho/NAA	2.49 ± 1.09	5.37 ± 2.81	0.010[b]
Q1-Q3	1.43-3.71	3.84-6.57	
Cho/Cr	2.44 ± 0.47	4.33 ± 1.77	0.016[b]
Q1-Q3	1.99-2.92	3.03-5.51	

MR, magnengic resonance; CBV, cerebral blood volume; CBF, cerebral blood flow; Cho, choline; NAA, n-acetyl aspartate; Cr, creatine. rCBV: relative cerebral blood volume, calculated by dividing the maximum value of the intratumor region by the contralateral normal white matter measured on CBV maps. rCBF: regional cerebral blood flow, calculated by dividing the maximum value of the intratumor region by the contralateral normal white matter measured on CBF maps. Cho/NAA: the ratio of choline to N-acetyl aspartate. Cho/Cr: the ratio of choline to creatine. Values are given as the mean ± SD; Q1-Q3: the 25th and 75th percentiles of measurements, *p*-values are significant for all pairs; [a]Comparisons were performed using the Chi-square test. [b]Comparisons were performed using the Mann-Whitney U test.

ROC curve analyses were performed to determine the ability of each parameter to distinguish BS-HGG from BS-LGG, as shown in Figures 4 and 5, and the AUC and Youden Index were calculated as presented in Table IV. The MRP values, consisting of the Cho/NAA (AUC: 0.944) and Cho/Cr ratios (AUC: 0.917; Figure 4), were better able to differentiate between BS-HGG and BS-LGG than the rCBF (AUC: 0.917), rCBV (AUC: 0.889; Figure 4), or age (AUC: 0.889; Figure 5).

Discussion

Our study included 7 children and 5 adults diagnosed with BSG, including 6 with high-grade tumors and 6 with low-grade tumors. A strong correlation was identified between age and malignancy, as the mean age of the BS-HGG group (14.8 ± 17.8 years) was significantly lower than that of the BS-LGG group (35.5 ± 22.9 years, $p = 0.024$), indicating that more malignant BSGs were more commonly diagnosed in children than in adults. Previous studies have also reported that pediatric cases diagnosed with BSG have a worse prognosis than adult cases diagnosed with BSG[1,5,6]. According to Reyes-Botero et al[5], among pediatric patients, grade IV is the most common BSG grade, accounting for 50%-60% of all pediatric BSG cases, whereas in adults, up to 80% of diffuse BSG cases are low-grade. However, other studies reported no association between age and histological grade. The study by Moharamzad et al[10] reported mean ages for BS-LGG and BS-HGG groups of 19 and 21, respectively ($p = 0.37$).

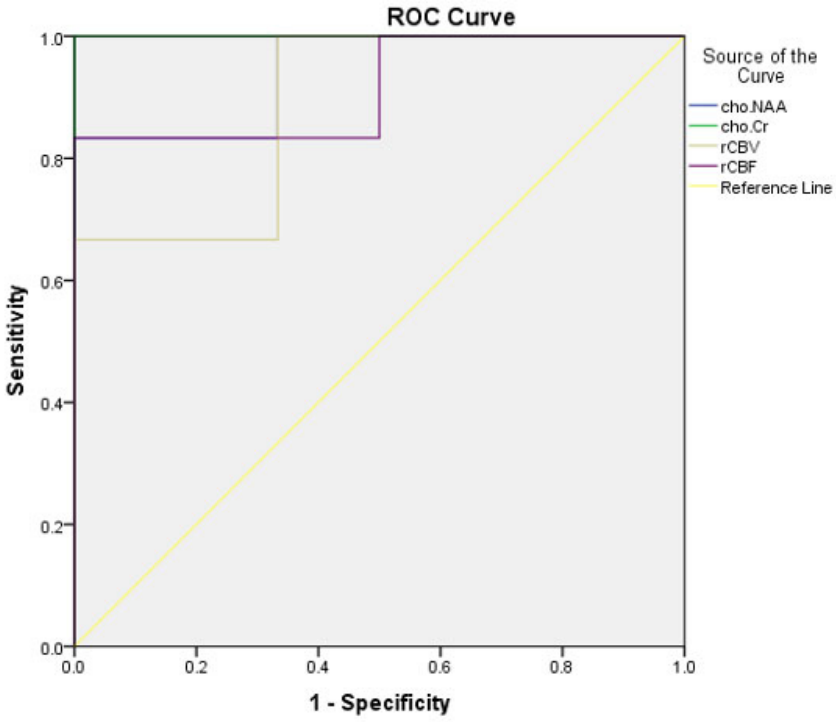

Figure 4. Receiver operating curve (ROC) analysis for relative cerebral blood volume (rCBV), regional cerebral blood flow (rCBF), choline (Cho)/N-acetyl aspartate (NAA), and Cho/creatine (Cr) for the distinction between high-grade brainstem glioma (BS-HGG) and low-grade brainstem glioma (BS-LGG). Because rCBF and Cho/NAA had the same Sp and Se values, the purple line is used for both.

Previous studies[9,10,12] examining the role of MRI in BSG grading have focused on the application of conventional MRI sequences. Imaging features including tumor location, tumoral extension into adjacent structures, enhancement characteristics, and necrosis have previously been reported to have diagnostic values for BSG grading. The study by Kwon et al[12] examining 20 BSG cases (15 high-grade tumors and 5 low-grade tumors) reported that 100% of high-grade tumors were located in the pons, whereas low-grade tumors were located in many locations. High-grade tumors caused diffuse brainstem enlargement, whereas low-grade tumors were often localized, and glioblastoma (grade IV) was often characterized by necrosis and ring enhancement. The study by Moharamzad et al[10] examining 96 BSG cases revealed that necrosis and heterogeneous enhancement are suggestive characteristics of BS-HGG. However, the correct diagnosis rate using conventional MRI sequences is not sufficient. Rachinger et al[9] examined 46 adult BSG cases and reported that the diagnostic Se and Sp of conventional MRI for identifying BS-LGG were only 62.5 and 46.6%, respectively, and

Table IV. The ROC parameters for discriminating BS-HGG from BS-LGG.

Parameter	AUC	Cutoff	Sensitivity	Specificity	Youden Index
Age	0.889	9.50[a]	100	83.3	0.833
rCBV	0.889	3.16[b]	100	66.7	0.667
rCBF	0.917	3.56[b]	83.3	100	0.833
Cho/NAA	0.944	3.88[b]	83.3	100	0.833
Cho/Cr	0.917	3.08[b]	83.3	100	0.833

ROC, receiver operating characteristic; BS-HGG, high-grade brainstem high-grade glioma; BS-LGG, low-grade brainstem glioma; AUC, area under the ROC curve; CBV, cerebral blood volume; CBF, cerebral blood flow; Cho, choline; NAA, n-acetyl aspartate; Cr, creatine. rCBV: relative cerebral blood volume, calculated by dividing the maximum value of the intratumor region by the contralateral normal white matter measured on CBV maps. rCBF: regional cerebral blood flow, calculated by dividing the maximum value of the intratumor region by the contralateral normal white matter that was measured on CBF maps. Cho/NAA: the ratio of choline to N-acetyl aspartate. Cho/Cr: the ratio of choline to creatine. [a]: Parameters for which values below the cutoff value suggest BS-HGG rather than BS-LGG. [b]: Parameters for which values above the cutoff value suggest BS-HGG rather than BS-LGG.

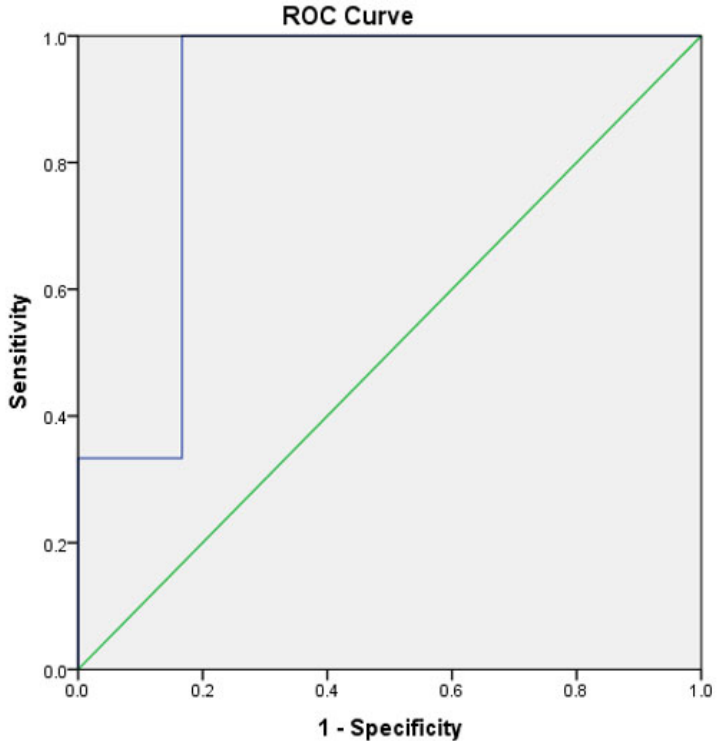

Figure 5. Receiver operating curve (ROC) analysis for age in the differentiation between high-grade and low-grade brainstem glioma. AUC = 0.889.

the corresponding values for BS-HGG were 58.3 and 61.7%, respectively. In the study by Goda et al[13], which included 20 BSG patients, the Se and Sp of conventional MRI for low-grade tumors were 66% and 33%, respectively, and the corresponding values for high-grade tumors were 50% and 50%, respectively. Conventional MRI has certain limitations when applied to BSG grading. Enhancement can be caused by both tumor angiogenesis and the disruption of the blood–brain barrier. In addition, many studies have shown that BS-HGGs may not enhance after contrast injection, whereas some BS-LGGs and non-tumor brainstem lesions may enhance after contrast injection[5,10,14,15]. For diffuse midline glioma, a BS-HGG with aggressive progression and overall survival of less than 1 year, contrast enhancement was only detected in 0%-25% of cases[1].

The application of MRP combined with MRS has the potential to overcome the limitations of conventional MRI. However, very few studies have examined the use of these two sequences for BSG grading. The only previous study examining these sequences in the literature was the study by Goda et al[13], which examined 20 BSG cases; however, only 8 cases had histopathological results, and the authors used the radiological prognostic index to classify tumors instead of histopathological grading. Our study used MRP and MRS for BSG grading and compared these outcomes with those based on pathological examinations for all 12 patients. This study is also the first to use ROC curve analysis to establish cutoff values for age, rCBV, rCBF, Cho/NAA, and Cho/Cre for use in BSG grading and diagnosis (Tables III and IV).

MRP assesses the extent of angiogenesis, which can provide a definitive diagnosis of brainstem tumors by differentiating tumors from non-tumor lesions and evaluating malignancy. Liu et al[16] studied the application of DSC perfusion to 16 cases of non-enhanced medullary lesions and showed that the maximum rCBV of BSG (1.56) was significantly higher than that of non-tumor lesions (0.5; $p < 0.001$). The study by Goda et al[13] revealed that MRP had Se and Sp values of 100% and 100%, respectively, for the diagnosis of BS-HGG, compared with the respective corresponding values of 50% and 50% for conventional MRI sequences. In our study, BS-LGG and BS-HGG had respective rCBV values of 2.77 ± 1.33 and 8.53 ± 6.21 ($p = 0.025$) and rCBF values of 2.27 ± 1.27 and 7.97 ± 4.67 ($p = 0.016$). Overall, the rCBV values for

BSG were significantly higher than those reported for general gliomas. In the study by Metellus et al[17], the mean rCBV of low-grade glioma was 0.84 ± 0.61. Many studies recommend using a cutoff rCBV value of 3 to differentiate between low-grade and high-grade glioma[18,19]. Jain et al[18] that an rCBV cutoff value of 3 had 97.2% Se and 100% Sp for glioma grading. In the present study, we performed BSG grading using an rCBV cutoff value of 3.16, which resulted in a Se of 100%, a Sp of 66.7%, and an AUC of 0.889; for rCBF, the cutoff value of 3.56 had a Se of 83.3%, a Sp of 100%, and an AUC of 0.917 (Table IV). The cutoff values for distinguishing BSG grades were generally higher than those reported for general gliomas[18,19].

MRS is a noninvasive diagnostic method capable of quantifying tumor tissue metabolism by measuring the concentrations of metabolites, which can be used to evaluate malignancy[20]. Low-grade glioma is often characterized by high concentrations of NAA, low concentrations of Cho, and the absence of lactate and lipid peaks. By contrast, high-grade glioma often shows low NAA levels due to neuronal degeneration or the destruction of neuronal structures in the tumor tissue. Glioblastoma (grade IV) is often characterized by necrosis with high concentrations of lipids and lactate peaks[20]. MRS performed on brainstem lesions has several challenges, including the proximity of bone, abundant vasculature, and the movement of cerebrospinal fluid, which can introduce heterogeneity in the primary magnetic field and difficult shimming[21]. However, Mascalchi et al[21] demonstrated that single-voxel MRS is clinically feasible for assessing lesions of the midbrain and pons. Previous studies also confirmed a role for MRS in the diagnosis of brainstem tumors. Smith et al[22] examined 34 patients with solitary brainstem lesions and reported that the Cho/Cr ratio in neoplastic lesions (2.0 ± 0.2) was significantly higher than that in non-neoplastic regions (1.4 ± 0.2). The study by Laprie et al[23] reported Cho/NAA and Cho/Cr ratios in pediatric patients with diffuse midline gliomas of 3.8 ± 0.93 and 3.55 ± 1.37, respectively, which were significantly higher than the ratios in the normal brain region ($p < 0.001$). Multivoxel MRS performed in our study revealed increased Cho/NAA and Cho/Cr ratios in all patients. The respective Cho/NAA and Cho/Cr ratios of BS-LGG cases were 2.49 ± 1.09 and 5.37 ± 2.81, whereas the ratios for BS-HGG cases were 2.44 ± 0.47 and 4.33 ± 1.77 (Table III). The Cho/NAA ratio has a better diagnostic ability for tumor grading than the Cho/Cr ratio ($p = 0.01$). This result is similar to a previous study by Salmaggi et al[6], which reported an increased Cho/Cr ratio in only 88.9% of cases, whereas 100% of cases were associated with an increased Cho/NAA ratio.

According to Law et al[24], glioma grading using a Cho/Cr cutoff value of 1.08 had a Se of 97.5% and a Sp of 12.5%, whereas a Cho/NAA cutoff value of 0.75 had a Se of 96.7% and an Sp of 10%. In the present study, we performed ROC curve analysis to establish appropriate cutoff values. A Cho/Cr cutoff value of 3.08 has 83.3% Se and 100% Sp for BSG grading, with an AUC of 0.917. A Cho/NAA cutoff value of 3.88 has 83.3% Se and 100% Sp for BSG grading, with an AUC of 0.944 (Table IV). The Cho/NAA ratio had the highest diagnostic value, followed by the Cho/Cr ratio, rCBF, and rCBV (Figure 1).

Limitations

Our study has some limitations. First, the small sample size could introduce bias in the assessment of diagnostic efficiency. Second, using multivoxel MRS for small lesions in the brainstem might influence metabolite concentrations, leading to inaccurate quantitative metabolite ratios. Last, BSG characteristics differ between adults and children, and the combined assessment of these two groups may affect the research results. Therefore, further studies using larger study populations and separate evaluations of adult and pediatric patients may improve the diagnostic accuracy of these measurements.

Conclusions

Our study indicates that rCBF, rCBV, and the Cho/NAA and Cho/Cre ratios obtained by comparing solid tumors with the normal brain parenchyma may be useful for differentiating between BS-LGG and BS-HGG. The combination of MRP and MRS can provide vital information for treatment planning and prognosis in patients with BSG.

Ethical Approval

Ethical clearance was received from the Institutional Ethics Committee of Hanoi Medical University (Ref: 634/GCN-HDDDNCYSH-DHYHN dated 16 March 2022).

Informed Consent

The informed consent of patients was waived.

Availability of Data and Material

The datasets generated and/or analysed during the current study are not publicly available due to privacy concerns but are available from the corresponding author on reasonable request.

Conflicts of Interest

The authors declare no conflict of interests.

Funding

This research received no external funding.

Authors' Contributions

D.-H. Nguyen and M.-D. Nguyen prepared, drafted, and revised the manuscript critically, for important intellectual content. D. Tran and D.-H. Nguyen contributed substantially to the acquisition, analysis, and interpretation of data. Each author gave final approval to the version of the manuscript submitted for publication and agreed to be accountable for all aspects of the work, ensuring that questions related to the accuracy or integrity of any part of the work are appropriately investigated and resolved.

ORCID ID

Nguyen Minh Duc: https://orcid.org/0000-0001-5411-1492.

References

1) Grimm SA, Chamberlain MC. Brainstem glioma: a review. Curr Neurol Neurosci Rep 2013; 13: 346.
2) Sarma A, Heck JM, Bhatia A, Krishnasarma RS, Pruthi S. Magnetic resonance imaging of the brainstem in children, part 2: acquired pathology of the pediatric brainstem. Pediatr Radiol 2021; 51: 189-204.
3) Flores MA, Blitz AM, Gujar SK, Huisman TAGM. (2020). Imaging of Brainstem Lesions. In: Jallo G, Noureldine M, Shimony N. (eds) Brainstem Tumors. Springer, Cham. doi.org/10.1007/978-3-030-38774-7_3
4) Louis DN, Perry A, Wesseling P, Brat DJ, Cree IA, Figarella-Branger D, Hawkins C, Ng HK, Pfister SM, Reifenberger G, Soffietti R, von Deimling A, Ellison DW. The 2021 WHO Classification of Tumors of the Central Nervous System: a summary. Neuro Oncol 2021; 23: 1231-1251.
5) Reyes-Botero G, Mokhtari K, Martin-Duverneuil N, Delattre JY, Laigle-Donadey F. Adult brainstem gliomas. Oncologist 2012; 17: 388-397.
6) Salmaggi A, Fariselli L, Milanesi I, Lamperti E, Silvani A, Bizzi A, Maccagnano E, Trevisan E, Laguzzi E, Rudà R, Boiardi A, Soffietti R; Associazione Italiana di Neuro-oncologia. Natural history and management of brainstem gliomas in adults. A retrospective Italian study. J Neurol 2008; 255: 171-177.
7) Leibetseder A, Leitner J, Mair MJ, Meckel S, Hainfellner JA, Aichholzer M, Widhalm G, Dieckmann K, Weis S, Furtner J, von Oertzen T, Preusser M, Pichler J, Berghoff AS. Prognostic factors in adult brainstem glioma: a tertiary care center analysis and review of the literature. J Neurol 2022; 269: 1574-1590.
8) Sun T, Xu Y, Pan C, Liu Y, Tian Y, Li C, Di F, Zhang L. Surgical treatment and prognosis of focal brainstem gliomas in children: A 7 year single center experience. Medicine (Baltimore) 2020; 99: e22029.
9) Rachinger W, Grau S, Holtmannspötter M, Herms J, Tonn JC, Kreth FW. Serial stereotactic biopsy of brainstem lesions in adults improves diagnostic accuracy compared with MRI only. J Neurol Neurosurg Psychiatry 2009; 80: 1134-1139.
10) Moharamzad Y, Sanei Taheri M, Niaghi F, Shobeiri E. Brainstem glioma: Prediction of histopathologic grade based on conventional MR imaging. Neuroradiol J 2018; 31: 10-17.
11) Sun T, Wan W, Wu Z, Zhang J, Zhang L. Clinical outcomes and natural history of pediatric brainstem tumors: with 33 cases follow-ups. Neurosurg Rev 2013; 36: 311-319; discussion 319-320.
12) Kwon JW, Kim IO, Cheon JE, Kim WS, Moon SG, Kim TJ, Chi JG, Wang KC, Chung JK, Yeon KM. Paediatric brain-stem gliomas: MRI, FDG-PET and histological grading correlation. Pediatr Radiol 2006; 36: 959-964.
13) Goda JS, Dutta D, Raut N, Juvekar SL, Purandare N, Rangarajan V, Arora B, Gupta T, Kurkure P, Jalali R. Can multiparametric MRI and FDG-PET predict outcome in diffuse brainstem glioma? A report from a prospective phase-II study. Pediatr Neurosurg 2013; 49: 274-281.
14) Dellaretti M, Touzet G, Reyns N, Dubois F, Gusmão S, Pereira JL, Blond S. Correlation among magnetic resonance imaging findings, prognostic factors for survival, and histological diagnosis of intrinsic brainstem lesions in children. J Neurosurg Pediatr 2011; 8: 539-543.
15) Yin L, Zhang L. Correlation between MRI findings and histological diagnosis of brainstem glioma. Can J Neurol Sci 2013; 40: 348-354.
16) Liu X, Kolar B, Tian W, Germin BI, Huang Y, Hu R, Zhong J, Ekholm S. MR perfusion-weighted imaging may help in differentiating between non-enhancing gliomas and nonneoplastic lesions in the cervicomedullary junction. J Magn Reson Imaging 2011; 34: 196-202.
17) Metellus P, Dutertre G, Mekkaoui C, Nanni I, Fuentes S, Ait-Ameur A, Chinot O, Dufour H, Figarella-Branger D, Cordoliani YS, Grisoli F. Intérêt de la mesure du volume sanguin régional cérébral relatif par IRM de perfusion dans la prise en charge des gliomes [Value of relative cerebral blood volume measurement using perfusion MRI in glioma management]. Neurochirurgie 2008; 54: 503-511.

18) Jain KK, Sahoo P, Tyagi R, Mehta A, Patir R, Vaishya S, Prakash N, Vasudev N, Gupta RK. Prospective glioma grading using single-dose dynamic contrast-enhanced perfusion MRI. Clin Radiol 2015; 70: 1128-1135.

19) Aprile I, Giovannelli G, Fiaschini P, Muti M, Kouleridou A, Caputo N. High- and low-grade glioma differentiation: the role of percentage signal recovery evaluation in MR dynamic susceptibility contrast imaging. Radiol Med 2015; 120: 967-974.

20) Bulik M, Jancalek R, Vanicek J, Skoch A, Mechl M. Potential of MR spectroscopy for assessment of glioma grading. Clin Neurol Neurosurg 2013; 115: 146-153.

21) Mascalchi M, Brugnoli R, Guerrini L, Belli G, Nistri M, Politi LS, Gavazzi C, Lolli F, Argenti G, Villari N. Single-voxel long TE 1H-MR spectroscopy of the normal brainstem and cerebellum. J Magn Reson Imaging 2002; 16: 532-537.

22) Smith JK, Londono A, Castillo M, Kwock L. Proton magnetic resonance spectroscopy of brainstem lesions. Neuroradiology 2002; 44: 825-829.

23) Laprie A, Pirzkall A, Haas-Kogan DA, Cha S, Banerjee A, Le TP, Lu Y, Nelson S, McKnight TR. Longitudinal multivoxel MR spectroscopy study of pediatric diffuse brainstem gliomas treated with radiotherapy. Int J Radiat Oncol Biol Phys 2005; 62: 20-31.

24) Law M, Yang S, Wang H, Babb JS, Johnson G, Cha S, Knopp EA, Zagzag D. Glioma grading: sensitivity, specificity, and predictive values of perfusion MR imaging and proton MR spectroscopic imaging compared with conventional MR imaging. AJNR Am J Neuroradiol 2003; 24: 1989-1998.